EXPERIMENT AND NUMERICAL SIMULATION ON TRANSIENT HEAT TRANSFER FROM SiC FOAM TO AIR-FLOW IN A HIGH TEMPERATURE TUBE

by

Xinlin XIA [a*], Xue CHEN [a,b*], Xiaolei LI [a], Bo LIU [a], and Yafen HAN [b]

[a] School of Energy Science and Engineering, Harbin Institute of Technology, Harbin, China
[b] School of Energy and Power Engineering, Northeast Electric Power University, Jilin, China

Original scientific paper
https://doi.org/10.2298/TSCI171103044X

In order to understand the high temperature heat transfer behavior of ceramic foam to air-flow, experiment and numerical simulation have been conducted for a tube fully filled with SiC foam under several air-flow velocities. The tested sample of SiC foam is characterized by a porosity of 0.88 and 10 pores per inch, which is heated to 1000 °C before the air-flow passes through. The transient temperature variation is recorded and discussed for several inlet air-flow velocities (2.9 m/s, 4.3 m/s and 5.8 m/s). Then, a computational model for the transient process is developed to numerically investigate the coupled radiative and convective heat transfer, and compared with the experimental data. The results show that the heat transfer reaches steady-state quickly and the time needed is less than 80 second. The transient deviation between the predicted and experimental data is less than 25.0%. Besides, it is found that there exists an obvious temperature difference between the fluid and solid phases, the maximum difference occurs at the neighbor region of tube wall and decreases as the inlet velocity increases at the steady-state.

Key words: *foam material, transient coupled heat transfer, high temperature, local thermal non-equilibrium*

Introduction

Foam materials present several promising characteristics which promote the extensive use in numerous thermal engineering applications. The coupled heat transfer within foam structure is crucial to the thermal performance of high temperature systems, such as porous burners [1] and solar receivers [2]. The thermal design, performance analysis and optimization essentially require the detailed and comprehensive knowledge on the heat transfer of foam-fluid system at high temperature.

Recently, many researchers have focused on the flow and heat transfer in foams with the thermal radiation neglected, and the effects of operation parameters are discussed theoretically and experimentally. For the high temperature conditions, however, thermal radiation may dominate the heat transfer process. Several simulations have been done to analyze the coupled radiative and convective heat transfer in such system. The local thermal equilibrium (LTE) model or the local thermal non-equilibrium (LTNE) model has been employed to characterize

*Corresponding authors, e-mail: Xiaxl@hit.edu.cn; Hit_chenxue@163.com

the heat exchange between the fluid and solid phases. The LTE model is mostly adopted, in which the two phases hold an identical temperature. Nield and Kuznetsov [3] investigated a combined conductive-convective-radiative heat transfer process in a channel occupied by a cellular porous medium. The influence of thermal radiation in a heated channel filled with metallic foam was evaluated by Andreozzi *et al*. [4] with radiative conductivity model. The coupled heat transfer inside a porous solar heat exchanger was studied by Rashidi *et al*. [5]. The coupled heat transfer problem was solved both semi-analytically and numerically by Dehghan *et al*. [6] to analyze the effects of porous medium shape parameter and radiation parameter on the thermal performance. Only a few numerical investigations used the LTNE model, taking the temperature difference between the two phases into account. Mahmoudi [7] studied the effect of thermal radiation on the temperature difference in a porous material subjected to isoflux boundary condition under steady-state. Chen *et al*. [8] discussed the influencing factors affecting the temperature difference in a transient heat transfer process inside an isothermal circular tube.

On the other hand, due to the extremely complex microstructure, Zhao [9] indicated that there has been scarcity in reliable experimental data for the open-cell foam in general. Besides, experiments on the flow and heat transfer in foams at high temperature could be very seldom found. Banerjee *et al*. [10] reported an study on a tube-in-tube heat exchanger filled with reticulated porous Al_2O_3 at temperature up to 1240 K. The flow and thermal behavior of Ni foam was tested as the volumetric receiver under concentrated solar radiation by Michailidis *et al*. [11].

From the review of literature, it can be seen that the high temperature coupled heat transfer in foams has not been adequately and comprehensively investigated, and experimental studies are especially rather limited. In this study, an experimental set-up is built to test the flow and heat transfer in a tube filled with SiC foam at high temperature. A numerical model is developed, the simulation is conducted and compared with the experimental data.

Experimental test rig

The experimental apparatus is schematically displayed in fig. 1. Air-flow is steadily supplied by the screw compressor, and flows into a clam chamber, then through the dehydrator to eliminate the water, oil and particulate materials. Volumetric flow rate is monitored by a flow meter with an accuracy of 1.0% rdg. Two valves (A and B) are used to alter the flow direction. The test section is made of stainless steel with an inner diameter of 50.0 mm, wall thickness of 1.5 mm, and length of 1.0 m. It is positioned inside of an open-ended furnace which can provide a high temperature environment up to 1100 °C. The foam specimen is inserted and positioned in the center of test section.

The test section and parameters measurement are depicted in fig. 2. Air temperatures at inlet and outlet are measured away from the foam specimen to avoid the effect of thermal radiation from the high temperature surface, using a *T*-type thermocouple (TC_1, junction diameter D_J = 0.5 mm, uncertainty of 0.5 K) and four *K*-type thermocouples (TC_{2-5}, D_J = = 1.0 mm, ±0.4%) respectively. The TC_{2-5} are arranged at r = 0, 6, 12, 18 mm, while TC_1 at the center of tube. Two *K*-type sheathed thermocouples (TC_6 and TC_7) are installed at the

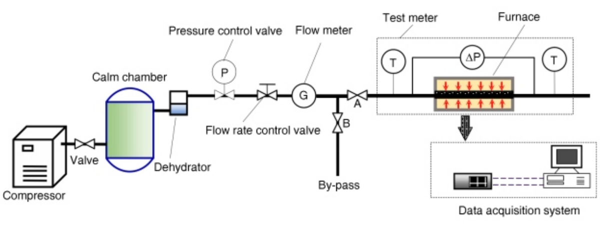

Figure 1. Schematic diagram of experimental apparatus

front and back center of foam specimen to monitor the temperature variation, while $TC_{8\text{-}10}$ for lateral temperature at x = 0.457, 0.5, 0.543 m. The temperature of tube wall outside the furnace is measured at equal spacing by $TC_{11\text{-}13}$ and $TC_{14\text{-}16}$, and TC_{17} and TC_{18} are used to record the wall temperature where the tube is not occupied by foam material. The wall temperature at the position where the outlet air temperature is measured is recorded by TC_{19}. The junction diameter of $TC_{11\text{-}19}$ (*K*-type) is 0.5 mm. Temperature distribution at the rear end of foam is obtained using an IR camera under the help of an infrared window with a transmissivity of 0.9. The pressure drop is measured using two differential pressure transmitters: one with an uncertainty of 0.08% full span (F.S.) (F. S. is 0-2.5 kPa), the other 0.0375% F. S. (F. S. is 0-100 kPa). Tube wall outside the furnace is thermally insulated. The foam specimen is made of SiC with 10 pores per inch (PPI) and a porosity of 0.88. The mean pore diameter, cell diameter and strut diameter are 2.535 mm, 5.537 mm and 0.913 mm, respectively, which are determined by image analysis using Image Pro-Plus software. Total length of SiC foam is 154 mm in the test.

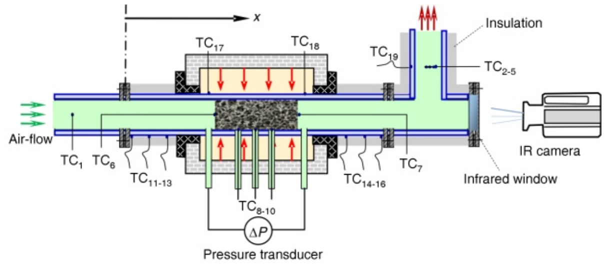

Figure 2. Schematic of the test section

First, turn on the valve B and turn off the valve A after a volumetric flow rate is obtained. Then, turn on the furnace and heat the foam specimen. Finally, alter the flow direction when the temperature of foam up to the desired and steady one, and here the heating temperature is set to 1000 °C. Subsequently, air-stream takes away the heat when passing through the foam skeleton. Volumetric air-flow rate, inlet and outlet fluid temperatures, and pressure drop have been measured with online data acquisition system. The pressure drop and temperature measurements start at the time air-flow entering the test section, and are acquired at 1.0 second interval until the steady-state is reached, while 10 second intervals for infrared image of end surface.

Numerical model

The test section can be divided to two regions: the clear fluid region at upstream and downstream (I), and the foam region (II). In the model, the curved segment at the outlet is neglected. Air-flow is assumed to be incompressible. Foam material is considered as a homogeneous, absorbing, emitting and isotropic scattering medium. There are two approaches to solve this kind of problem: one-domain approach and two-domain approach [12]. The former is adopted here, which considers the porous foam as a pseudo-fluid and the composite region as a continuum, automatically ensuring the momentum and energy continuity at the interface. The *k*-*ε* turbulent model is adopted in the fluid region, and the non-Darcy model is used to demonstrate the flow behavior inside the porous region [13]. The LTNE model is employed, considering the temperature difference between the two phases. The conservation equations of mass, momentum, and energy are given, respectively:

$$\frac{\partial(\phi\rho_{\mathrm{f}})}{\partial\tau} \quad (\rho_{\mathrm{f}}\mathbf{U}) \quad 0 \tag{1}$$

$$\frac{1}{\phi}\frac{\partial(\rho_{\mathrm{f}}\mathbf{U})}{\partial\tau} \quad \frac{1}{\phi} \quad \rho_{\mathrm{f}}\frac{\mathbf{U}\,\mathbf{U}}{\phi} \qquad p \qquad \frac{\mu_{\mathrm{e}}}{\phi} \quad \mathbf{U} \qquad \delta\mathbf{F} \tag{2}$$

$$\frac{\partial(\phi\rho_{\mathrm{f}}c_{\mathrm{f}}T_{\mathrm{f}})}{\partial\tau} \quad (\rho_{\mathrm{f}}c_{\mathrm{f}}\mathbf{U}T_{\mathrm{f}}) \quad (\lambda_{\mathrm{fe}} \quad T_{\mathrm{f}}) \quad \delta h_v(T_{\mathrm{s}} \quad T_{\mathrm{f}}) \tag{3}$$

$$\delta\,\frac{\partial[(1 \quad \phi)\rho_{\mathrm{s}}c_{\mathrm{s}}T_{\mathrm{s}}]}{\partial\tau} \quad (\lambda_{\mathrm{se}} \quad T_{\mathrm{s}}) \quad h_v(T_{\mathrm{f}} \quad T_{\mathrm{s}}) \quad S_r \quad 0 \tag{4}$$

where $\mathbf{U}$ is air-flow velocity, ρ and c are, respectively, the density and specific heat, p – the pressure, τ – the flow time, μ_{e} – the effective dynamic viscosity, $\mathbf{F}$ – the momentum source caused by the insert of foam, λ_{fe} and λ_{se} are effective thermal conductivities, h_{v} – the volumetric heat transfer coefficient, and S_{r} – the radiative source. Some parameters in the model are determined:

$$\text{region I: } \phi \quad 1.0,\ \delta \quad 0,\ \mu_{\mathrm{e}} \quad \mu_{\mathrm{f}} \quad \mu_{\mathrm{t}},\ \lambda_{\mathrm{fe}} \quad \lambda_{\mathrm{f}} \quad \lambda_{\mathrm{t}}$$

$$\text{region II: } \phi \quad 0.88,\ \delta \quad 1,\ \mu_{\mathrm{e}} \quad \mu_{\mathrm{f}},\ \lambda_{\mathrm{fe}} \quad \phi\lambda_{\mathrm{f}},\ \lambda_{\mathrm{se}} \quad (1 \quad \phi)\lambda_{\mathrm{s}}/3$$

where μ_{t} and λ_{t} are the turbulent viscosity and turbulent thermal conductivity, respectively. The equations of turbulent kinetic energy and the rate of energy dissipation based on the k-ε turbulent model are:

$$\frac{\partial(\rho_{\mathrm{f}}k)}{\partial\tau} \quad (\rho_{\mathrm{f}}k\mathbf{U}) \quad \mu_{\mathrm{f}} \quad \frac{\mu_{\mathrm{t}}}{\sigma_{\mathrm{k}}} \quad k \quad G_k \quad \rho_{\mathrm{f}}\varepsilon \tag{5}$$

$$\frac{\partial(\rho_{\mathrm{f}}\varepsilon)}{\partial\tau} \quad (\rho_{\mathrm{f}}\varepsilon\mathbf{U}) \quad \mu_{\mathrm{f}} \quad \frac{\mu_{\mathrm{t}}}{\sigma_{\varepsilon}} \quad \varepsilon \quad \frac{\varepsilon}{k}(C_1C_{\mathrm{k}} \quad C_2\rho_{\mathrm{f}}\varepsilon) \tag{6}$$

where G_{k} is the production of turbulence energy, $C_1 = 1.44$, $C_2 = 1.92$, σ_{k} , and σ_{ε} . The radiative transfer equation is solved by the P1 radiation model. The transport equation of incident radiation, G, can be expressed:

$$\frac{1}{3(\kappa_a \quad \kappa_s)} \quad G \quad \kappa_a(4\sigma T_s^4 \quad G) \tag{7}$$

Thus, the radiative source term can be computed as $S_r \quad \kappa_a(4\sigma T_{\mathrm{s}}^4 \quad G)$. Based on the geometric optics approximation, the radiative properties of foam are determined [14]:

$$\kappa_a \quad 1.5\varepsilon_p(1 \quad \phi)/d_{\mathrm{p}} \tag{8}$$

$$\kappa_s \quad 1.5(1 \quad \varepsilon_p)(1 \quad \phi)/d_{\mathrm{p}} \tag{9}$$

where ε_p is the foam emissivity, κ_a and κ_a are the absorption coefficient and scattering coefficient, respectively.

So far, many investigations have been done to study the flow and heat transfer characteristics in foam materials, in order to determine the source term, $\mathbf{F}$, and volumetric heat transfer coefficient, h_v. However, still no correlation is able to predict the two main inputs with sufficient accuracy [15, 16]. Therefore, for the specific foams, a series of tests are necessary. The volumetric heat transfer coefficient can be determined from experiment using a single-blow technique. The authors have proposed a correlation from experimental data of several foams (Cu, Ni, and SiC, 0.87 ϕ and 10-40 PPI), as reported in [17].

$$\mathrm{Nu}_{\mathrm{v}} \quad 0.34\phi^{\ 2}\,\mathrm{Re}_d^{0.61}\,\mathrm{Pr}^{1/3} \tag{10}$$

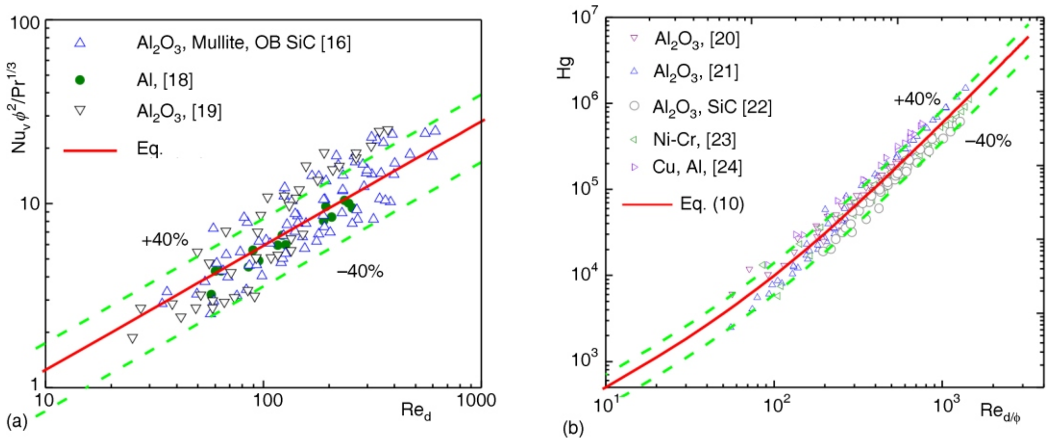

Figure 3. Comparison of results predicted from correlations and those from literature; (a) volumatric heat transfer coefficient, (b) pressure drop

where $Nu_v \quad h_v d_p^2/\lambda_f$, $Re_d \quad \rho_f u d_p/\mu_f$ and $20 \quad Re_d \quad 10^3$. From the comparison in fig. 3(a), it is found that most of the experimental data from literature fall within an error of 40%. The pressure drop across foam material can be described as Forchheimer equation $\Delta p / L \quad u\mu_f / k_1 \quad \rho_f u^2 / k_2$, where the coefficients k_1 and k_2 can be determined by measurement at different velocities and structural parameters. Similarly, the authors have performed several tests using the foams in [17], and derived a correlation:

$$\frac{\Delta p}{L} \quad \frac{44.5}{\phi d_p^2}\mu_f u \quad \frac{0.55}{\phi^2 d_p}\rho_f u^2 \tag{11}$$

A comparison is displayed in fig. 3(b), where Hg is Hagen number [$Hg \quad \Delta p \rho_f d_p^3/(L\mu_f^2)$] and $20 \quad Re_d/\phi \quad 2800$. The maximum error is about 40%. Therefore, the momentum source in eq. (2) can be written as $\mathbf{F} \quad 44.5\mu_f U/(\phi d_p^2) \quad 0.55\rho_f |\mathbf{U}|\mathbf{U}/(\phi^2 d_p)$.

Thermal properties of foam are assumed to be constant, λ_s = 80 W/(mK), c_s = 1244 J/(kgK), and $\rho_s \quad 3210$ kgm^3. The emissivity is ε_p . Air is regarded as ideal gas and the viscosity is calculated through Sutherland law. The thermal capacity and conductivity can be described:

$$c_p \quad 1.93 \quad 10 \quad ^{10}T_f^4 \quad 8 \quad 10 \quad ^7T_f^3 \quad 1.14 \quad 10 \quad ^3T_f^2 \quad 4.49 \quad 10 \quad ^1T_f \quad 1.06 \quad 10^3 \tag{12}$$

$$\lambda_f \quad 1.52 \quad 10 \quad ^{11}T_f^3 \quad 4.86 \quad 10 \quad ^8T_f^2 \quad 1.02 \quad 10 \quad ^4T_f \quad 3.93 \quad 10 \quad ^3 \tag{13}$$

Air-flow enters the tube at a uniform temperature and velocity. The tube is opened to ambient at exit cross section ($p = 0$, with reference pressure 101325 Pa). The tube wall in region II is subjected to a variable radiative flux from the high temperature furnace which is set to 1000 °C. The emissivities of tube wall and inner surface of furnace are 0.8 and 1.0, respectively. Due to the heat transport from the tube inside the furnace along axial direction, tube wall in region I is set as wall temperature boundary changing with time. The wall temperature is fitted from $TC_{11\text{-}13}$ or $TC_{14\text{-}16}$ in the region outside the furnace, while the temperature is given by TC_{17} or TC_{18} for the region inside the furnace. The initial temperature in foam is chosen as the average temperature of $TC_{6\text{-}10}$. A 2-D axisymmetric model is built and FLUENT is used to solve the governing equations. The grid independence is guaranteed when grid number is 250 × 40. Convergence is reached if the residuals are below 10^{-7}.

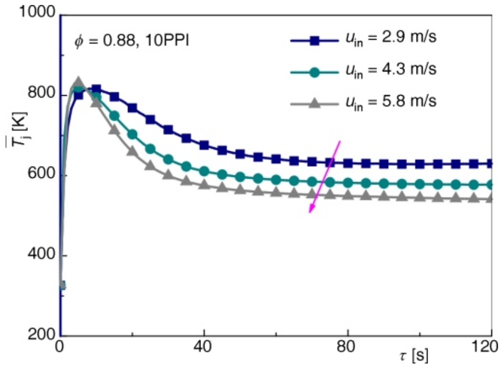

Figure 4. Variation of $\overline{T}_J$ with time at different inlet velocities

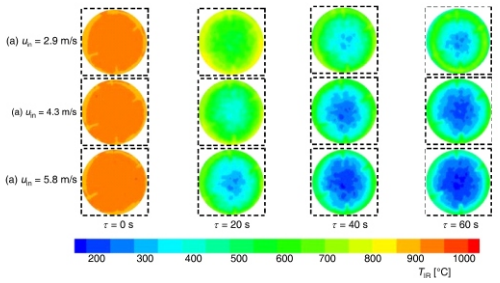

Figure 5. Blackbody equivalent temperature of the end surface of foam

Results and discussion

Three sets of experiments are conducted with different inlet air velocities (2.9, 4.3, and 5.8 m/s). The transient outlet air temperature is difficult to obtain directly from the correction of thermocouple temperature, since the accurate time dependent flow velocity and thermo-physical properties can not be measured. Moreover, temperature variations of TC_{2-5} reflect the variation of outlet air temperature. The average temperature of TC_{2-5} ($\overline{T}_J$) is plotted in fig. 4. It can be seen that the temperature has a noticeable change when τ 50 second, three processes almost reach the steady-state when τ 80 second, and the time needed slightly decreases as the inlet velocity increases, nearly 75, 71, and 66 seconds for the three tests, respectively. The temperature $\overline{T}_J$ at u_{in} = 2.9 m/s is 88.5 K higher than that at u_{in} = 5.8 m/s under the steady-state condition.

The IR camera is calibrated to give maps of blackbody equivalent temperature as shown in fig. 5. The temperature has a nearly uniform distribution at τ = 0 second, as the non-uniformity is less than 3.0%. The temperature of foam decreases greatly with the increasing of time at the central region, due to the higher heat transfer rate from foam skeleton to air-flow than that from tube wall to air-flow. Besides, the temperature is lower when inlet velocity increases at the same time, for the reason that the volumetric heat transfer coefficient increases as the velocity increases.

Due to the rapid variation in the flow and temperature fields during the transient process and the thermal properties and velocity at outlet can not be precisely estimated, a correction of the transient outlet air temperature directly from the experimental data can not be performed. Thus, the comparison is made on the thermocouple temperature at outlet to check the validity of simulation. The numerical thermocouple temperature at outlet is calculated based on the energy balance analysis. The heat loss caused by conduction is neglected, as the main factor is the thermal radiation from tube wall. The heat balance equation of the thermocouple can be expressed:

$$\rho_J c_J V_J \frac{dT_J}{d\tau} \quad hA_J(T_f \quad T_J) \quad \sigma\varepsilon_J A_J(T_w^4 \quad T_J^4) \tag{14}$$

where A_J is the surface area of thermocouple junction, ε_J – the emissivity of junction surface, T_w – the tube wall temperature which is measured by TC_{19}, σ – the Stefan-Boltzmann constant, and h – the convective heat transfer coefficient which can be evaluated by:

$$h \quad [2.0 \quad (0.4\,\mathrm{Re}_J^{1/2} \quad 0.06\,\mathrm{Re}_J^{2/3})\,\mathrm{Pr}^{0.4}]k_f / D_J \tag{15}$$

where Re_J $\rho_f u D_J/\mu_f$, ε_J 0.6, and D_J = 1.0 mm. Thermal properties of junction are ρ_J = = 8665 kg/m^3, c_J = 486 J/(kgK), and λ_J W/(mK^{-1}). The average temperature of TC_{2-5} is compared in fig. 6, where the deviation is defined as $\zeta \;\; \left|\overline{T}_{\mathrm{J,NUM}} \;\; \overline{T}_{\mathrm{J,EXP}}\right| / \overline{T}_{\mathrm{J,EXP}} \;\; 100\%$. The same variation trends are observed. Since the volumetric heat transfer coefficient becomes larger at a higher velocity, the thermocouple temperature increases more quickly at a high velocity. The steep change in the initial time period is due to the thermal inertia of thermocouple, and the deviation increases with time and then reaches the maximum which are 25.0%, 18.2%, and 12.8% at u_{in} = 2.9,4.3,5.8 m/s, respectively. As the time increases, the deviation increases again after a decrease. The deviations at the steady-state are 6.3%, 13.8%, and 19.8% for the three tests, respectively. Additionally, a comparison of pressure drop at steady-state is made (see tab. 1). It indicates that the maximum deviation is 8.8%, where the deviation is defined as $\zeta_p \;\; \left|\Delta p_{\mathrm{NUM}} \;\; \Delta p_{\mathrm{EXP}}\right| / \Delta p_{\mathrm{EXP}} \;\; 100\%$. The previous comparisons demonstrate an acceptable agreement between the measured and predicted values.

Figure 7 illustrates the transient temperature variation at x = 0.5 m for τ second and inlet velocity of 2.9 m/s. It presents a rapid change in temperature and considerable temperature difference between the fluid and solid phases. Besides, the temperature difference de-

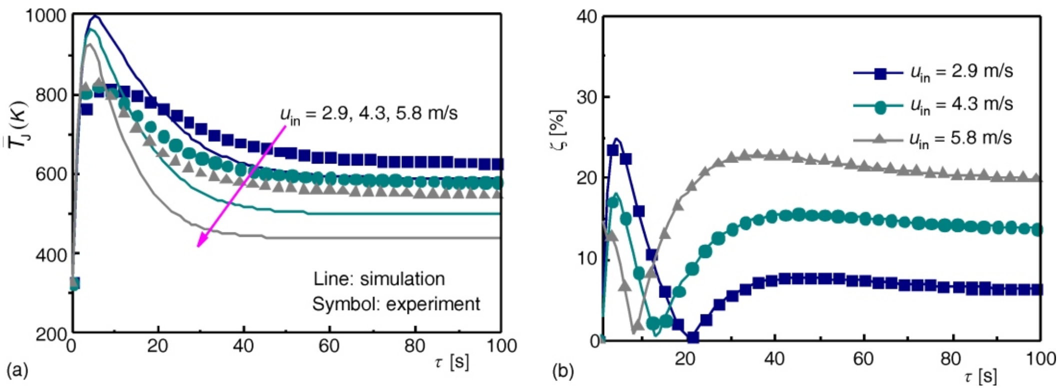

Figure 6. Comparison of numerical and experimental results at different inlet velocities; (a) average thermocouple temperature at outlet, (b) deviation between experiment and simulation

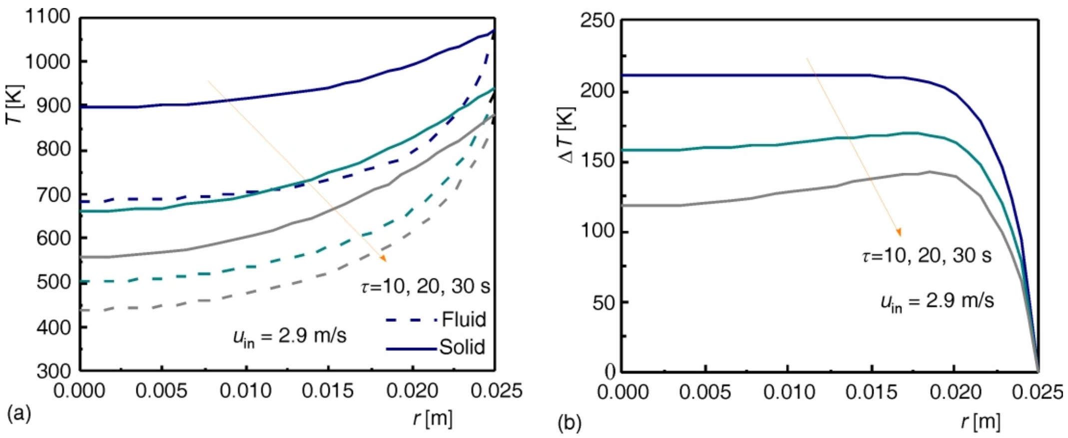

Figure 7. Temperature distribution at x = 0.5 m for τ = 10, 20, 30 s; (a) temperature distribution, (b) temperature difference

Table 1. Comparison of the pressure drop at steady-state

u_{in} [ms^{-1}]	p_{EXP} [Pa]	Δp_{NUM} [Pa]	ζ_p[%]
2.9	1053	971	7.8
4.3	1825	1664	8.8
5.8	3020	2808	7.0

creases as the flow time increases. The maximum difference are 211.7 K, 169.4 K, and 141.9 K, respectively.

For the steady-state, temperature distributions at cross sections $x = 0.5$ m and $x = = 0.577$ m (end surface of foam) are presented in fig. 8. As can be seen from the figure, the temperature decreases noticeably with the increasing of inlet velocity. The temperature difference between the fluid and solid phases has an obvious reduction when the inlet velocity increases, as shown in fig. 9. For example, the temperature difference on the axis decreases from 85.5 K to 42.4 K as the velocity increases from 2.9 m/s to 5.8 m/s. The maximum temperature differences which almost occur at the near wall region (around the position $r = 0.02$ m) for $u_{in} = 2.9$, 4.3, 5.8 m/s are 119.7 K, 114.4 K, and 109.8 K, respectively. The solid temperature near tube wall is higher due to the heated wall, and low velocity near the wall causes low heat transfer rate, which leads to a large temperature difference.

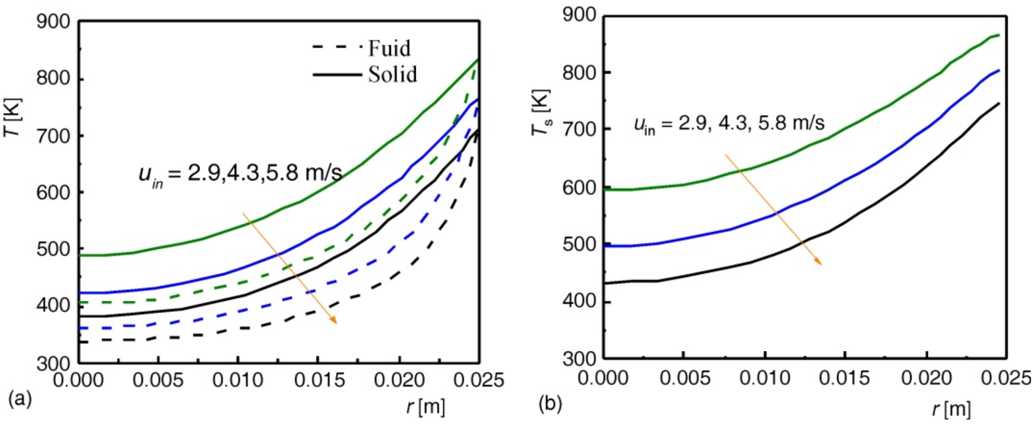

Figure 8. Comparison of temperature distribution under the steady-state; (a) x = 0.5 m, (b) x = 0.577 m (end surface)

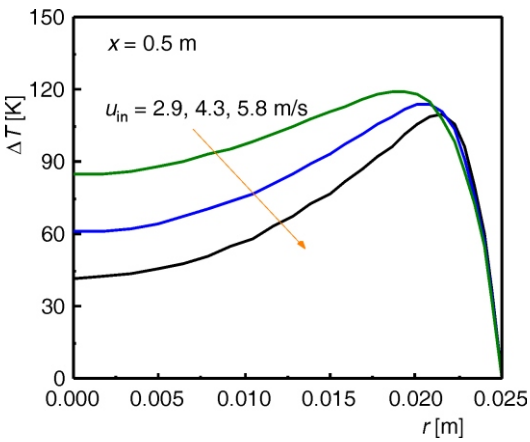

Figure 9. Temperature difference between two phases under the steady-state

Conclusions

An experiment apparatus is built to investigate the coupled heat transfer in foam material at high temperature. A SiC foam is tested under three different inlet velocities (2.9 m/s, 4.3 m/s, and 5.8 m/s), and the transient temperature data are obtained until the steady-state is reached.

The time to steady-state is almost less than 80 second, which slightly decreases as the inlet velocity increases. The temperature in the center region of end surface of the foam specimen decreases as the inlet velocity increases. A numerical model is developed to simulate the heat transfer and compared with the experiment. New correlations of volumetric heat transfer coefficient and pressure drop are proposed and used in the simulation. A maximum deviation of 25.0 % is found between the predicted and experimental data during the whole transient process. Besides, it is found that the maximum temperature difference occurs at the near wall region (around the position $r = 0.02$ m), and decreases with the increasing of inlet velocity. Thus, the LTNE model is strongly recommended for the thermal analysis of such high temperature applications of foam materials.

Acknowledgment

This work is supported by the National Natural Science Foundation of China (No. 51536001, 51606034).

Nomenclature

A – surface area, [m^2]
c – specific heat, [Jkg^{-1}K^{-1}]
D – diameter, [m]
d_p – pore diameter, [mm]
F – source term of momentum equation
Hg – Hagen number, [–]
h – heat transfer coefficient, [Wm^{-2}K^{-1}]
h_v – volumetric heat transfer coefficient, [Wm^{-3} K^{-1}]
k – turbulent kinetic energy, [m^{2}s^{-2}]
L – length, [m]
Nu$_v$ – volumetric Nusselt number, [–]
p – pressure, [Pa]
Re – Reynolds number, [–]
S_r – radiative source term, [Wm^{-3}]
T – temperature, [K]
U – superficial velocity, [ms^{-1}]
u – velocity [ms^{-1}]
x, r – co-ordinates in flow region, [m]

Greek symbols

ε – dissipation rate of the turbulent kinetic energy, [m^{2}s^{-3}]
ε_p – foam emissivity, [–]
ε_J – junction emissivity, [–]
κ_a – absorption coefficient, [m^{-1}]
κ_s – scattering coefficient, [m^{-1}]
λ – thermal conductivity, [Wm^{-1}K^{-1}]
μ – dynamic viscosity, [kgm^{-1}s^{-1}]
ρ – density, [kgm^{-3}]
ϕ – porosity, [–]

Subscripts

e – effective
f – fluid
in – inlet
j – junction
s – solid
w – wall

References

[1] Mujeebu, M. A., *et al.*, Applications of Porous Media Combustion Technology – A Review, *Applied Energy, 86* (2009), 9, pp. 1365-1375
[2] Gomez-Garcia, F., *et al.*, Thermal and Hydrodynamic Behavior of Ceramic Volumetric Absorbers for Central Receiver Solar Power Plants: A Review, *Renewable and Sustainable Energy Reviews, 57* (2016), May, pp. 648-658
[3] Nield, D. A., Kuznetsov, A. V., Forced Convection in Cellular Porous Materials: Effect of Temperature-Dependent Conductivity Arising from Radiative Transfer, *International Journal of Heat and Mass Transfer, 53* (2010), 13-14, pp. 2680-2684
[4] Andreozzi, A., *et al.*, Numerical Analysis of Radiation Effects in a Metallic Foam by Means of the Radiative Conductivity Model, *Applied Thermal Engineering, 49* (2012), Dec., pp. 14-21
[5] Rashidi, S., *et al.*, Heat Transfer Enhancement and Pressure Drop Penalty in Porous Solar Heat Exchangers: A Sensitivity Analysis, *Energy Conversion and Management, 103* (2015), Oct., pp. 726-738
[6] Dehghan, M., *et al.*, Convection-Radiation Heat Transfer in Solar Heat Exchangers Filled with a Porous Medium: Homotopy Perturbation Method versus Numerical Analysis, *Renewable Energy, 74* (2015), Feb., pp. 448-455

[7] Mahmoudi, Y., Effect of Thermal Radiation on Temperature Differential in a Porous Medium under Local Thermal Non-Equilibrium Condition, *International Journal of Heat and Mass Transfer, 76* (2014), Sept., pp. 105-121
[8] Chen, X., *et al.*, Transient Thermal Analysis of the Coupled Radiative and Convective Heat Transfer in a Porous Filled Tube Exchanger at High Temperatures, *International Journal of Heat and Mass Transfer, 108* (2017), Part B., pp. 2472-2480
[9] Zhao, C. Y., Review on Thermal Transport in High Porosity Cellular Metal Foams with Open Cells, *International Journal of Heat and Mass Transfer, 55* (2012), 13-14, pp. 3618-3632
[10] Banerjee, A., *et al*., Experimental Investigation of a Reticulated Porous Alumina Heat Exchanger for High Temperature Gas Heat Recovery, *Applied Thermal Engineering, 75* (2015), Jan., pp. 889-895
[11] Michailidis, N., *et al*., Flow, Thermal and Structural Application of Ni-Foam as Volumetric Solar Receiver, *Solar Energy Materials and Solar Cells, 109* (2013), Feb., pp. 185-191
[12] Goyeau, A., *et al*., Momentum Transport at a Fluid-Porous Interface, *International Journal of Heat and Mass Transfer, 46* (2003), 21, pp. 4071-4081
[13] Amori, K. E., Laibi, H. A., Experimental and Numerical Analysis of Electrical Metal Foam Heater, *Energy, 36* (2011), 7, pp. 4524-4530
[14] Vafai, K., *Handbook of Porous Media,* 2nd ed., Porland, Taylor and Francis, Oxford, UK, 2005
[15] Edouard, D., *et al*., Pressure Drop Modeling on Solid Foam: State-of-the-Art Correlation, *Chemical Engineering Journal, 144* (2008), 2, pp. 299-311
[16] Dietrich, B., Heat Transfer Coefficients for Solid Ceramic Sponges-Experimental Results and Correlation, *International Journal of Heat and Mass Transfer, 61* (2013), June, pp. 627-637
[17] Xia, X.L., *et al*., Experiment on the Convective Heat Transfer from Airflow to Skeleton in Open-Cell Porous Foams, *International Journal of Heat and Mass Transfer, 106* (2017), Mar., pp. 83-90
[18] Hwang, J. J., *et al*., Measurement of Interstitial Convective Heat Transfer and Frictional Drag for Flow across Metal Foams, *Journal of Heat Transfer, 124* (2002), 1, pp. 120-129
[19] Younis, L. B., Viskanta, R., Experimental Determination of the Volumetric Heat Transfer Coefficient between Stream of Air and Ceramic Foam, *International Journal of Heat and Mass Transfer, 36* (1993), 6, pp. 1425-1434
[20] Incera Garrido, G., *et al*., Mass Transfer and Pressure Drop in Ceramic Foams: a Description for Different Pore Sizes and Porosities, *Chemical Engineering Science, 63* (2008), 21, pp. 5202-5217
[21] Dietrich, B., *et al*., Pressure Drop Measurements of Ceramic Sponges-Determining the Hydraulic Diameter, *Chemical Engineering Science, 64* (2009), 16, pp. 3633-3640
[22] Akbar Shakiba, S., *et al*., Experimental Investigation of Pressure Drop through Ceramic Foams: an Empirical Model for Hot and Cold Flow, *Journal of Fluids Engineering, 133* (2011), 11, pp. 101-105
[23] Medraj, M., *et al*., The Effect of Microstructure on the Permeability of Metallic Foams, *Journal of Materials Science, 42* (2007), June, pp. 4372-4383
[24] Kamath, P. M., *et al*., Convection Heat Transfer from Aluminium and Copper Foams in a Vertical Channel-an Experimental Study, *International Journal of Thermal Sciences, 64* (2013), Feb., pp. 1-10

Paper submitted: November 3, 2017
Paper revised: November 26, 2017
Paper accepted: November 26, 2017